Optical Limiting Properties of Zinc- and Platinum-Based Organometallic Compounds

Alexander Baev, Oscar Rubio-Pons, Faris Gel'mukhanov, and Hans Ågren*

Theoretical Chemistry, Roslagstullsbacken 15, AlbaNova, Royal Institute of Technology, S-106 91 Stockholm, Sweden

Received: January 28, 2004

Optical power limiting is theoretically studied using an approach that combines quantum electronic structure calculations of multiphoton excitations and classical calculations of dynamical wave propagation. We illustrate the capability of such a combined approach by presenting results for a couple of organometallic compounds; basic metal−base porphyrins, vinylphenylamine porhyrin, and the so-called type IVc platinum compound. A comparative analysis of their electronic properties related to nonlinear absorption of electromagnetic radiation and their optical limiting capability has been performed based on dynamical simulations of the nonlinear pulse propagation taking account of resonant as well as off-resonant effects. Several key features and rate-limiting steps in the transmission have been examined in relation to various characteristics of the pulse. It is found that the resonant vs off-resonant conditions, the saturation conditions and the dephasing play critical roles for the nonlinear transmission. The saturation effects are sensitive to the pulse duration, the inter-system crossing rate and the quenching of the higher triplet state. The inter-system crossing rate has to be comparable with the inverse pulse duration in order to boost the stepwise two-photon channel associated with singlet−singlet followed by triplet−triplet transitions. It is illustrated that structure-to-property relations of the rate-limiting steps serve as important criteria for choices of compounds suitable for the application of interest.

I. Introduction

Organometallic compounds have attracted a large amount of attention in a variety of fundamental and applied photonic research areas, involving optical control, light harvesting, and photosynthetic processes. They are considered as some of the most promising materials for applications in a wide range of areas such as quantum electronics, optical power limiting, biological imaging, and photodynamic therapy, to mention a few of many examples.[1−8] Metal−base porphyrins and many compounds based on platinum exhibit strong nonlinear optical (NLO) properties attributed mainly to the two-photon absorption (TPA) process.[9,10] Much theoretical effort has been undertaken in this area with the goal to model the interaction of NLO materials with intense laser beams in order to screen candidate compounds and to predict materials with especially large two-photon absorption cross sections. Thus, modeling of the photophysics of organometallic compounds has become of fundamental interest to understand and design NLO devices.

However, as is well established, in addition to the conventional coherent one-step two-photon process, which nowadays readily can be treated by means of electronic structure calculations, there are a number of processes that one has to account for in order to obtain a measure of the actual capability of the material for a particular NLO response or for light control in general. For instance, the competition of the resonant coherent one-step channel with many-step, often off-resonant, channels was recently elucidated by the present authors[11] and found to be very crucial for optical power limiting (OPL) by condensed materials for which decoherence processes in general are fast. Apart from the dephasing of the singlet excited state (S_1), the competition between the coherent one-step and incoherent many-step channels were found delicately dependent on pulse intensity, pulse length and excitation frequency. The role of saturation and the hierarchy of saturation intensities of the different excitations was also found to be of importance, especially in the case of long-pulse excitations. That is to say that two-photon absorption, even with proper account of desaturating excited state absorption, can in many cases not be the sole source of, for instance, a good optical limiting capability. In particular, for solutions, one needs to account for the above-mentioned dephasing broadening of resonances, which then probably becomes the main medium effect for the TPA as well as for the OPL property.

Both excited-state absorption (S_1-S_n) and inter-system (S_1-T_1) crossing should in principle be taken into account as being main desaturation channels, the balance between the two being quite system dependent. However, strong such channels leads to a shift of the rate-limiting bottleneck further on in the chain, to triplet−triplet absorption, and to quenching of the excited states, either S_n or T_n. In principle, the complete, so-called, Jablonsky diagram should be mastered, involving excitations and couplings within and between the singlet and triplet manifold of states. The calculations of all the contributing processes and steps easily become a formidable undertaking, and although recent developments of quantum modeling of nonlinear properties and multiphoton excitations have taken big steps forward to solve these challenges—n.b. through development of time-dependent density functional theory for linear and nonlinear interactions[12] paralleled by fully relativistic response theory[10]—it is still of great importance to find simplifying rules and structure−property relations and to pinpoint the rate-limiting steps for an efficient material in the context of optical power limiting. The present work can be viewed as an attempt to address these problems by capitalizing on recent accomplishments on both the quantum and the classical sides of the problem of light control, that is quantum computations of all important

10.1021/jp040078s CCC: $27.50
Published on Web 08/13/2004

legs involved in the Jablonsky diagram, respectively, dynamic pulse propagation accounting for the various characteristics of the laser beam.

In the present work, we attempt to take account of the theoretical accomplishments briefly reviewed above and study a few organometallic complexes that recently have been brought to the fore as good candidates for optical limiting. Thus, along with the basic metal−base porphyrins and zinc−base porphyrin with an attached push−pull system (vinylphenylamine Zn−base porphyrin) we have analyzed a platinum compound called IVc with designed charge-transfer enhanced nonlinear absorption cross-section.[10,14] Photon absorption in these compounds involves both the ground-state singlet−singlet and the excited-state triplet−triplet channels. The relative contributions of those channels, their appearance and mutual competition as well as their allover NLO and OPL properties are comparatively analyzed in some detail in this paper.

The presentation is organized as follows. We review the essentials of the density matrix and field equations describing our modeling approach in section II. The details of electronic structure calculations and of dynamics simulations are outlined in section III. The main analysis and the discussion of the results obtained are given in section IV, and our findings are summarized in in the last section, section V.

II. Theory

We consider the nonlinear interaction of the optical field

$$\mathbf{E} = \frac{\mathcal{E}}{2} e^{-\imath\omega t + \imath kz} + \text{c.c.} \tag{1}$$

with a many-level molecule. The polarization of the medium has the same structure:

$$\mathbf{P} = \mathrm{Tr}(\mathbf{d}\rho) = \sum_{\beta\alpha} \mathbf{d}_{\beta\alpha}(t)\rho_{\alpha\beta} = \mathcal{P} e^{-\imath\omega t + \imath kz} + \text{c.c.} \tag{2}$$

To know the polarization we need the transition dipole moments, $\mathbf{d}_{\beta\alpha}(t) = \mathbf{d}_{\beta\alpha} \exp(i\omega_{\alpha\beta}t)$, and the density matrix, $\rho_{\alpha\beta}$, of the medium. Here, $\omega_{\alpha\beta} = (E_\alpha - E_\beta)/\hbar$, is the frequency of the transition $\alpha \rightarrow \beta$.

We make the reasonable approximation of having slowly varying phases and amplitudes: $\omega \gg |\dot{\mathcal{E}}/\mathcal{E}|$; $k \gg |\partial \ln \mathcal{E}/\partial z|$. The substitution of **E** (1) and **P** (2) in Maxwell's equations and a selection of contributions with the frequencies ω results in the following paraxial wave equations for the amplitude of the field:

$$\left(\frac{\partial}{\partial z} + \frac{1}{c}\frac{\partial}{\partial t} - \frac{\imath}{2k}\Delta_\perp\right)\mathcal{E} = \frac{\imath k}{\epsilon_0}\mathcal{P} \tag{3}$$

The SI system of units is used here.

The density matrix equation for nonlinear media reads

$$\left(\frac{\partial}{\partial t} + \hat{\Gamma}\right)\rho = \frac{\imath}{\hbar}[\rho, V],\ \mathrm{Tr}\rho = N,\ V = \mathbf{E}\cdot\mathbf{d} \tag{4}$$

where the concentration of the absorbing molecules is denoted by N, and $\hat{\Gamma}$ is the relaxation matrix. The kinetic equations for populations, $\rho_{\alpha\alpha}$, and off-diagonal elements, $\rho_{\alpha\beta}$, of the density matrix read as follows:

$$\left(\frac{\partial}{\partial t} + \Gamma_{\alpha\beta}\right)\rho_{\alpha\beta} = \delta_{\alpha,\beta}\sum_{\gamma>\alpha}\Gamma^\alpha_\gamma\rho_{\gamma\gamma} + \frac{\imath}{\hbar}\sum_\gamma(\rho_{\alpha\gamma}V_{\gamma\beta} - V_{\alpha\gamma}\rho_{\gamma\beta}) \tag{5}$$

Here we neglect the space derivatives at the left-hand side of the kinetic equations which are responsible for the Doppler effect ($\exp(\pm\imath kz) \rightarrow 1$). The Doppler broadening in the studied condensed absorber is indeed negligible compared to the dephasing rate, $\Gamma_{\alpha\beta}$. Because of nonradiative conversion the rate Γ^α_β of decay transitions $\beta \rightarrow \alpha$ is large in organic molecules and almost completely coincides with the total decay rate $\Gamma_{\alpha\alpha}$.

The decay rate of the αth level is the sum of the partial decay rates of this level to all lower levels

$$\Gamma_{\alpha\alpha} = \sum_{\beta(<\alpha)}\Gamma^\beta_\alpha \tag{6}$$

We seek the solution of the density matrix equations making use of the Fourier expansion:

$$\rho_{\alpha\beta} = e^{\imath\omega_{\alpha\beta}t}[r_{\alpha\beta} + \sum_{n=1}^{\infty}(r^{(n)}_{\alpha\beta}\, e^{-\imath n\omega t} + r^{(n)*}_{\beta\alpha}\, e^{\imath n\omega t})] \tag{7}$$

This representation is a key step to solve the problem of propagation of a strong pump field through a nonlinear many-level medium. Substitution of the Fourier expansion (eq 7) yields the following equations for populations ($\alpha = \beta$) and polarizations ($\alpha \neq \beta$):[11]

$$\begin{aligned}
&\left(\frac{\partial}{\partial t} + \imath\omega_{\alpha\beta} + \Gamma_{\alpha\beta}\right)r_{\alpha\beta} = \delta_{\alpha\beta}\sum_{\gamma(>\alpha)}\Gamma^\alpha_\gamma r_{\gamma\gamma} + \imath\sum_\gamma[(r^{(1)}_{\alpha\gamma} + \\
&\qquad r^{(1)*}_{\gamma\alpha})G_{\gamma\beta} - G_{\alpha\gamma}(r^{(1)}_{\gamma\beta} + r^{(1)*}_{\beta\gamma})],\\
&\left(\frac{\partial}{\partial t} + \imath(\omega_{\alpha\beta} - \omega) + \Gamma_{\alpha\beta}\right)r^{(1)}_{\alpha\beta} = \delta_{\alpha\beta}\sum_{\gamma(>\alpha)}\Gamma^\alpha_\gamma r^{(1)}_{\gamma\gamma} + \\
&\qquad \imath\sum_\gamma[(r_{\alpha\gamma} + r^{(2)}_{\alpha\gamma})G_{\gamma\beta} - G_{\alpha\gamma}(r_{\gamma\beta} + r^{(2)}_{\gamma\beta})],\\
&\left(\frac{\partial}{\partial t} + \imath(\omega_{\alpha\beta} - n\omega) + \Gamma_{\alpha\beta}\right)r^{(n)}_{\alpha\beta} = \delta_{\alpha\beta}\sum_{\gamma(>\alpha)}\Gamma^\alpha_\gamma r^{(n)}_{\gamma\gamma} + \\
&\qquad \imath\sum_\gamma[\,(r^{(n-1)}_{\alpha\gamma} + r^{(n+1)}_{\alpha\gamma})G_{\gamma\beta} - G_{\alpha\gamma}(r^{(n-1)}_{\gamma\beta} + r^{(n+1)}_{\gamma\beta})]
\end{aligned} \tag{8}$$

Here $n \geq 2$ and $G_{\alpha\beta} = \mathcal{E}\cdot\mathbf{d}_{\alpha\beta}/2\hbar$. The parts in eq 8 are solved self-consistently together with the wave equation for the intensity $I = c\epsilon_0|\mathcal{E}|^2/2$:

$$\left(\frac{\partial}{\partial z} + \frac{1}{c}\frac{\partial}{\partial t}\right)I = 2\hbar\omega\,\mathcal{I}m\sum_{\beta\alpha}G_{\beta\alpha}r^{(1)}_{\alpha\beta} \tag{9}$$

III. Outlines of Numerical Simulations

As a prerequisite for the dynamical simulations we first computed transition energies, the permanent and transition dipole moments with the Gaussian98[15] and Dalton[16] quantum chemistry packages. The results were then used to model the medium of interest and to simulate nonlinear pulse propagation. For some of the molecules we also computed two-photon transition matrix elements in order to evaluate the coherent one-step contribution to the total nonlinear absorption cross section. That was done by means of the Dalton program. In our simulations, we ignored the role of vibrational degrees of freedom (for a discussion of vibrationally induced TPA, we refer to ref 34).

A. Electronic Structure Calculations. The parametrizations of the calculations chosen for display in the present work, that is geometries, functionals and basis sets, follow experience and precalculations of the present and other compounds which we have conducted along with the development and use of the Dalton code and use of the Gaussian code. Details of these

considerations are available from the authors upon request. The results shown in figures and tables of the paper are due to the following particularities: The ground-state geometries for all compounds were optimized making use of Gaussian98 program at the B3LYP/6-31G* level. The triplet state geometries were optimized at the same B3LYP/6-31G* level. The ground-state absorption spectra were calculated making use of TD-DFT linear response (DFT-LR) with the cc-pVDZ basis set. The transition dipole moments between the excited states, two-photon absorption transition matrix elements, and triplet−triplet absorption were calculated making use of TD-DFT quadratic response (DFT-QR) implemented in the Dalton program. For the Zn−base, Mg−base, Pb−base, and free-base porphyrins, these calculations were performed with the hybrid functional B3LYP, with the cc-pVDZ basis set for the C, N, and H atoms, and with atomic natural orbitals (ANO) basis set.[17] For Zn and Mg atoms, the following contraction was used: Zn (21s15p10d) contracted to [5s3p2d] and Mg (17s12p5d) contracted to [5s3p2d]. In the case of Pb−base porphyrin, an effective core potential (ECP) was used to describe the absorption spectrum.

In the case of vinylphenylamine Zn−base porphyrin (ZnPP) and IVc platinum-based compound (PtC), the properties of interest were computed with Gaussian98[15] at the B3LYP/LANL2DZ level for PtC and B3LYP/6-31G(d,p) for ZnPP. The excited-state absorption for these compounds was modeled by means of single-excitation configuration interaction (CI-singles) method, and the permanent dipole moments were calculated by making use of the finite field gradients technique.

B. Dynamics Simulations. We performed the simulations of nonlinear propagation of a laser pulse through the media consisting of dissolved organometallic compounds: Zn−base porphyrin, ZnPP, and PtC, making use of our recently developed code based on the theory represented by eqs 8 and 9 and described in detail in refs 11 and 18. As demonstrated in those papers the devised approach allows for a good quantitative estimation of the nonlinear transmission. The solvent was modeled by a dephasing rate taken as high as 0.01−0.1 eV.[11,35] Small off-resonant absorption by the solvent is neglected as it takes place in the region below 300 nm.[1,3] The decay rates of the selected states of the compounds of interest are collected in Tables 5−7. The estimation of these are somewhat involved: We first estimated the radiative decay rates making use of the calculated transition dipole moments. The nonradiative decay rates are quite problematic to be estimated, so for the full decay rates, we used the orders of magnitude which are characteristic for the given class of organometallics. We account for that the full decay rate of a state is just the sum of partial decay rates to all lower states: $\Gamma_{ii} = \sum_{j<i} \Gamma_i^j$ (this is the reason for the appearance of numbers like 0.9999 in Tables 5−7).

IV. Results and Discussion

A. Electronic Structure Calculations. We remind the reader that numerous theoretical studies of different porphyrins have been carried out. In recent years the emphasis has shifted from semiempirical calculations[19,20] to more sophisticated ab initio wave function and, in particular, density functional theory (DFT) approaches.[21−26] Nakatsuji et al. applied symmetry-adapted-cluster (SAC) and SAC−CI (configuration interaction) methods to free-base porphyrins (FBP)[21] and to a number of porphyrin-type molecules[22,27] in order to interpret the singlet−singlet absorption spectrum. Rubio and Serrano-Andrés[28,29] have calculated the singlet−singlet absorption spectra of those compounds making use of the CASPT2. Time-dependent DFT has also been applied recently to electronic absorption spectra of FBP in many studies.[24−26,30−32]

TABLE 1: Selected Relative Excitation Energies (ΔE, eV) and Transition Dipole Moments (μ_i, au) of the Low-Lying Singlet States of Zinc−Base, Manganese−Base, Lead−Base, and Free-Base Porphyrins, of Vinylphenylamine Zinc−Base Porphyrin (ZnPP), and of the IVc Pt Compound (PtC)

molecule	state	$\Delta E_{\mathrm{DFT-LR}}$[a]	μ_x	μ_y	μ_z
FBP	1^1B_{3u}	2.270	0.0004	0.0004	
	1^1B_{2u}	2.427			
	2^1B_{3u}	3.314	1.6259	−1.6259	
	2^1B_{2u}	3.487	1.9415	1.9415	
	3^1B_{3u}	3.748	1.6486	1.6486	
	3^1B_{2u}	3.848	2.0227	−2.0227	
ZnP	1^1E_u (S_1)	2.435	0.2098	−0.2098	
	2^1E_u (S_2)	3.541	3.2483	3.2483	
	1^1B_{1g} (S_3)	3.727			
	3^1E_u (S_4)	3.836	−0.8546	0.8546	
	4^1E_u (S_5)	4.289	1.2761	1.2761	
MgP	1^1E_u	2.380	0.1165	0.1165	
	2^1E_u	3.500	−3.2651	−3.2651	
	1^1B_{1g}	3.756			
	3^1E_u	3.774	0.7440	0.7440	
	4^1E_u	4.235	−1.4980	−1.4980	
PbP	1^1S	1.741			
	4^1S	2.329	−0.2024	0.0023	−0.0060
	9^1S	3.436		−0.1367	0.0052
	11^1S	3.528	1.5214	−0.5035	−0.0013
	12^1S	3.537	1.2840	0.0052	−1.9132
	13^1S	3.538	−1.9040	0.2727	−1.2713
ZnPP	1^1S (S_1)	2.131	−3.1416	0.0002	0.0687
	3^1S (S_2)	2.760	0.0024	−0.6188	0.0001
	4^1S (S_3)	2.829	−3.4248	−0.0016	−0.0302
	5^1S	2.882	−2.3244	0.0023	−0.0437
	6^1S (S_4)	2.908	0.0010	1.6859	
PtC	$2^1A'$ (S_1)	2.760	5.4870	−0.0046	
	$3^1A'$ (S_2)	3.165	−0.0017	−0.2255	
	$4^1A'$ (S_3)	3.341	−0.0561	−1.7405	
	$5^1A'$	3.579	2.3778	−0.1819	

[a] Absorption at the equilibrium ground-state geometry. [b] The labels in parentheses correspond to the labeling throughout the text.

TABLE 2: Selected Absolute Excitation Energies (ΔE, eV) and Transition Dipole Moments (μ_i, au) of the Low-Lying Triplet States of ZnP, ZnPP, and PtC

molecule	state	$\Delta E_{\mathrm{DFT-QR}}$[a]	μ_x	μ_x	μ_x
ZnP	1^3B_{1u} (T_1)	1.775			
	1^3B_{3g} (T_2)	3.215	0.3027	−0.3027	
	2^3B_{3g}	3.301	0.0098		
	2^3B_{2g}	3.301		−0.0098	
	1^3A_u	4.965			
ZnPP	$^3T_1$ (T_1)	1.573			
	$^3T_2$	1.800	−0.0739		−0.0275
	$^3T_4$ (T_2)	2.587	2.0997		−0.0677
	$^3T_6$ (T_3)	3.150	−4.5893		0.0011
PtC	$^3T_1$ (T_1)	2.170			
	$^3T_2$	2.997	−0.7633	−0.0692	
	$^3T_4$ (T_2)	3.357	4.7255	0.0520	
	$^3T_8$	4.010	2.2486	0.4219	

[a] Absorption at the equilibrium lowest triplet state geometry [b] The labels in parentheses correspond to the labeling in Tables 6 and 7.

The absorption spectra of the singlet states of porphyrins have thus been extensively studied theoretically,[13,24,25,28,29] in particular, magnesium and free-base porphyrins. On the other hand, absorption and emission associated with triplet channels have not attracted attention to a comparable extent, despite that triplet excited states of photosynthetic pigments are known to be involved in photosynthesis and similar photochemical reaction cycles.[33] The triplet state energies addressed by Nakatsuji et al.[21] and Sundholm[24] have to our knowledge not been complemented by studies of singlet−triplet transition cross sections. Recently, the present authors[37] used the response function technique for triplet excitations[12] developed at our laboratory

TABLE 3: Two-Photon Absorption Tensor (S_{ij}, au) of Zinc−Base, Manganese−Base, Lead−Base, and Free-Base Porphyrins

molecule	state	ΔE_{DFT-QR}[a]	S_{xx}	S_{yy}	S_{zz}	S_{xy}	S_{xz}	S_{yz}
FBP	2^1A_g	3.404	1.6	−1.6				
	3^1A_g	3.586	−8.6	−8.6				
	4^1A_g	4.031	81.3	81.3				
	1^1B_{1g}	4.255				−95.2		
ZnP	2^1A_g	3.768	−1.3	1.3				
	3^1A_g	3.977	−17.5	−17.5				
	2^1B_{1g}	3.893				21.2		
	2^1E_g	6.735					−4.7	−4.7
MgP	1^1B_{1g}	3.758				−21.9		
	2^1A_g	3.800	−2.8	2.8				
	3^1A_g	4.004	−18.1	18.1				
	2^1E_g	6.231					−1.9	−1.9
PbP	$^1S_2$	1.989	1.9	1.9	−39.4			
	$^1S_3$	2.329					2.9	
	$^1S_4$	2.329						2.9
	$^1S_5$	2.909					11.4	
	$^1S_6$	2.909						11.4

[a] Absorption at the equilibrium ground-state geometry.

TABLE 4: Permanent Dipole Moments and Excited State Absorption (μ_{ij}, au) of the Singlet and Triplet States for Zinc−Base, Manganese−Base, and Free-Base Porphyrins

molecule	matrix element	x	y	z
ZnP	$\langle 1\,^1E_u\|d\|\,1^1B_{1g}\rangle$	−0.2944	−0.2944	
	$\langle 2\,^1E_u\|d\|\,1^1B_{1g}\rangle$	−0.1932	0.1932	
	$\langle 3\,^1E_u\|d\|\,1^1B_{1g}\rangle$	0.9505	0.9505	
	$\langle 4\,^1E_u\|d\|\,1^1B_{1g}\rangle$	1.0233	−1.0233	
	$\langle 1\,^1E_u\|d\|\,1^1E_u\rangle$	−0.3400	0.3400	
	$\langle 2\,^1E_u\|d\|\,2^1E_u\rangle$	−0.3600	0.3600	
	$\langle 1^3A_u\|d\|\,1^3B_{1g}\rangle$			0.0304
	$\langle 1^3A_u\|d\|\,1^3B_{2g}\rangle$		−0.8546	
	$\langle 1^3A_u\|d\|\,1^3B_{3g}\rangle$	−0.8546		
ZnPP	$\langle ^1S_0\|d\|\,^1S_0\rangle$		−0.8120	
	$\langle ^1S_1\|d\|\,^1S_1\rangle$	0.0735	0.0735	
	$\langle ^3T_1\|d\|\,^3T_1\rangle$		−0.9060	
	$\langle ^1S_1\|d\|\,^1S_3\rangle$	7.3231		0.0292
	$\langle ^1S_4\|d\|\,^1S_3\rangle$	−5.6759		0.0853
	$\langle ^1S_5\|d\|\,^1S_3\rangle$	−7.9856		0.0397
	$\langle ^1S_6\|d\|\,^1S_4\rangle$	−8.0916		0.0546
	$\langle ^1S_6\|d\|^1S_5\rangle$	6.2083		−0.0329
PtC	$\langle 1^1A'\|d\|\,1^1A'\rangle$	0.1092	0.6978	
	$\langle 2^1A'\|d\|\,2^1A'\rangle$	1.0657	−0.1837	
	$\langle 3^1A'\|d\|\,3^1A'\rangle$	1.3965	0.8452	
	$\langle ^3T_1\|d\|\,^3T_1\rangle$	0.4747	−0.8676	
	$\langle ^3T_3\|d\|\,^3T_3\rangle$	4.3364	0.9187	
	$\langle 2^1A'\|d\|\,3^1A'\rangle$	−14.0607	0.1503	
	$\langle 3^1A'\|d\|\,5^1A'\rangle$	18.1245	−0.1238	

[a] Absorption at the equilibrium ground-state geometry.

to characterize the triplet state, viz. absorption cross sections, phosphorescence rates, zero-field splittings and **g**-tensors.[37] This development matches well the fact that porphyrin-based dyes have been recognized as very promising for designing nonlinear optical devices[9,32] something we capitalize upon in the present study.

The electronic absorption of metal−base porphyrins exhibit some common trends. For instance, the linear absorption spectra of porphyrins are dominated by two intense bands, commonly named Q and B bands. The Q band is mainly centered at about 2 eV and the B band is near the UV region at about 3 eV. Both Q and B bands are created by $\pi \rightarrow \pi^*$ transitions. Other transitions with less intensity, bands N and L, are in the region of 3.6 and 4.3 eV, respectively. For the Q band the absorption is rather weak while it is much more intense for the B band. In the free-base porphyrin where the metal is substituted by two hydrogen atoms, the most remarkable feature is the splitting of the Q band due to the loss of symmetry (from D_{4h} to D_{2h}[25,28]). For the triplet states in metal−base porphyrins a distorted geometry is expected because of the Jahn−Teller effect. For instance, in the case of Zn−base porphyrin possessing D_{4h} symmetry in the ground state the Jahn−Teller effect leads to D_{2h} symmetry. This feature makes the symmetry assignment of the lowest triplet state rather unclear, depending on the host or solvent.[9]

Summarizing the data extracted from the previous papers and obtained from our computations we can say that Mg− and Zn−base porphyrins have molecular symmetry D_{4h} at the equilibrium ground-state geometry; the inclusion of a heavier metal atom such as Pb breaks the symmetry to C_{4v}. Our calculations of the Q and B bands of Mg− and Zn−base porphyrins are in good agreement with previous theoretical calculations although we use smaller basis sets in the present work. The origin of the B band is the doublet 2^1E_u state which gives the most intense transition in the spectra (Table 1). The Q band of free-base porphyrin is split because of two states—1^1B_{3u} and 1^1B_{2u}—which are responsible for this band. The lack of the metal−base and lower molecular symmetry in free-base porphyrin makes the first excited-state lower in energy and less intense in the linear absorption spectrum. The oscillator strengths of 1^1B_{2u}, 1^1B_{3u} states are rather small, in accordance with weak intensities seen in the experimental spectrum.[31] The energies of the Q bands are a little higher in our calculations than reported in the experimental works (see tables and citations in ref 31).

The study of TPA has been carried out for the Zn−base, Mg−base, Pb−base, and free-base porphyrins. The largest values of the TPA transition matrix elements were found for free-base porphyrin at 4.03 and 4.26 eV (Table 3) owing to the large value of the dipole transition matrix element from the ground state to the 3^1B_{2u} and 3^1B_{3u} states with the energies 3.75 and 3.85 eV, respectively (Table 1). The intense excited-state absorption from these states to the 1^1B_{1g} and 4^1A_g states, which are forbidden in one-photon absorption spectra, give then the high values of the TPA tensor. In Mg−, Pb−, and Zn−base porphyrins, the dipole transition matrix elements in the B band are not so intense as in free-base porphyrin; instead, intensity is shifted to the Q band. It results in small values of the TPA transition matrix elements. Among the unsubstituted metalloporphyrins, we have focused on the Zn member in our pulse simulations.

Attachment of substituents enhances both linear and nonlinear absorption of porphyrins due to the better charge separation. Our calculations of the ZnPP molecule confirmed this clearly (see Tables 1, 2, and 4). However, the energy of the lowest excited singlet becomes lower—2.13 eV—compared with 2.45 eV for the basic Zn−base porphyrin. Thus, using the lower frequency of the exciting radiation the two-photon resonance with this state is fulfilled. This idea is applicable to PtC: The linear absorption in the basic P−Pt−P unit of this compound is weak as shown by Norman et al.[10] However, the inclusion of strongly absorbing groups such as phenyl and thiophene enhances the linear and nonlinear absorption.

We also studied an alternative mechanism of TPA enhancement in this work based on the stepwise two-photon processes going through the triplet manifold of states which can be the source of large values of the TPA cross section. $\pi \rightarrow \pi^*$ transitions to the 3.22 eV triplet state in ZnP, to the 3.15 eV triplet state in ZnPP, and to the 3.36 eV triplet state in the PtC molecule dominate in the spectra of triplet−triplet absorption (see Table 2). The fast inter-system crossing (ISC) then drives the nonlinear absorption. The efficiency of this kind of TPA is affected both by the ISC rate and the pulse duration (see

TABLE 5: Decay Rates of ZnP, s^{-1}

	S_0	S_1	S_2	S_3	T_1	T_2
S_1	0.01×10^9	1.0×10^{10}			9.99×10^9	
S_2	0.70×10^{10}	9.00×10^{10}	1.00×10^{11}		0.1×10^{10}	0.20×10^{10}
S_3	4.90×10^{11}	1.50×10^{12}	3.00×10^{12}	5.00×10^{12}	0.05×10^{11}	0.05×10^{11}
T_1	1.00×10^6				1.00×10^6	
T_2	0.50×10^9	0.50×10^9			9.00×10^9	1.00×10^{10}

TABLE 6: Decay Rates of ZnPP, s^{-1}

	S_0	S_1	S_2	S_3	S_4	T_1	T_2	T_3
S_1	4.00×10^8	1.00×10^9				6.00×10^8		
S_2	0.09×10^{10}	9.90×10^{10}	1.00×10^{11}			0.01×10^{10}		
S_3	0.4999×10^{11}	0.50×10^{11}	9.00×10^{11}	1.00×10^{12}	0.0001×10^{11}			
S_4	0.099×10^{11}	0.40×10^{11}	1.50×10^{11}	8.00×10^{11}	1.00×10^{12}	0.0005×10^{11}	0.0005×10^{11}	
T_1	1.00×10^6					1.00×10^6	-	
T_2	0.05×10^9	0.05×10^9				9.90×10^9	1.00×10^{10}	
T_3	0.0001×10^{11}	0.0001×10^{11}	0.0001×10^{11}	0.0003×10^{11}	0.0004×10^{11}	2.999×10^{11}	7.00×10^{11}	1.00×10^{12}

TABLE 7: Decay Rates of PtC, s^{-1}

	S_0	S_1	S_2	S_3	T_1	T_2
S_1	0.1×10^{10}	1.00×10^{11}			9.90×10^{10}	
S_2	0.0999×10^{10}	9.90×10^{10}	1.00×10^{11}		0.0001×10^{10}	
S_3	0.9999×10^{11}	1.00×10^{11}	7.9999×10^{11}	1.00×10^{12}	0.0001×10^{11}	0.0001×10^{11}
T_1	1.00×10^6				1.00×10^6	
T_2	0.005×10^{12}	0.005×10^{12}	0.01×10^{12}		9.98×10^{12}	1.00×10^{13}

discussion below). Thus, for ZnPP and PtC molecules a stronger nonlinear optical response is expected as they have larger ground-state and excited-state absorption cross sections compared to basic metal−base porphyrins. Moreover, lower symmetry removes symmetry restrictions giving rise to different nonlinear absorption channels contributing to the total nonlinear absorption cross section.

B. Dynamics. *1. Zn−Base Porphyrin.* The Zn−base porphyrin molecule is shown in Figure 2. The energy level scheme is given in Figure 1. One can here discern three possible two-photon absorption channels tuning the radiation frequency in two-photon resonance with either of the S_1, S_2, or S_3 singlet states. It is instructive to look closer at these channels to select the important mechanism. If we tune the radiation frequency in resonance with the singlet S_1 there are three two-photon absorption paths starting at S_0 and finishing at S_1: $\langle S_0|S_2\rangle\langle S_2|S_1\rangle$, $\langle S_0|S_3\rangle\langle S_3|S_1\rangle$, and $\langle S_0|S_1\rangle(\langle S_1|S_1\rangle - \langle S_0|S_0\rangle)$. The S_1-S_2 and S_0-S_3 transitions are symmetry forbidden, which results in strong suppression of the first two paths (see Tables 1 and 4). The last channel involving the permanent dipole moments of the two lowest singlets is very weak according to Table 1.

Tuning the radiation frequency in resonance with the singlet S_2 state initiates three two-photon absorption paths starting at S_0 and finishing at S_2: $\langle S_0|S_3\rangle\langle S_3|S_2\rangle$, $\langle S_0|S_1\rangle\langle S_1|S_2\rangle$, and $\langle S_0|S_2\rangle(\langle S_2|S_2\rangle - \langle S_0|S_0\rangle)$. The first two channels are again suppressed by symmetry reasons. The last channel can be quite intense because of the large value of the transition dipole moment between the singlets S_0 and S_2 (see Table 1). On the other hand, we will have a one-photon absorption channel S_0-S_1 in this case which, even being off-resonant, can dominate over the two-photon absorption channel until the saturation of the transition S_0-S_1 is reached.

Finally, if the radiation frequency is tuned in resonance with the singlet S_3, three two-photon absorption paths starting at S_0 and finishing at S_3 emerge: $\langle S_0|S_1\rangle\langle S_1|S_3\rangle$, $\langle S_0|S_2\rangle\langle S_2|S_3\rangle$, and $\langle S_0|S_3\rangle(\langle S_3|S_3\rangle - \langle S_0|S_0\rangle)$. The last channel is here suppressed because the dipole transition S_0-S_3 is symmetry forbidden. Of the two remaining channels the second one—$\langle S_0|S_2\rangle\langle S_2|S_3\rangle$—seems to be more efficient according to Tables 1 and 4. From the outline above, it seems appropriate to tune the radiation frequency in two-photon resonance with the S_0-S_2 or S_0-S_3 transitions in our simulations. The dephasing rate was set to 0.1 eV. The concentration of porphyrin molecules in solution—another important parameter—was set to 1×10^{19} cm^{-3}. The length of the cell was chosen to be 3 mm. As the molecule is

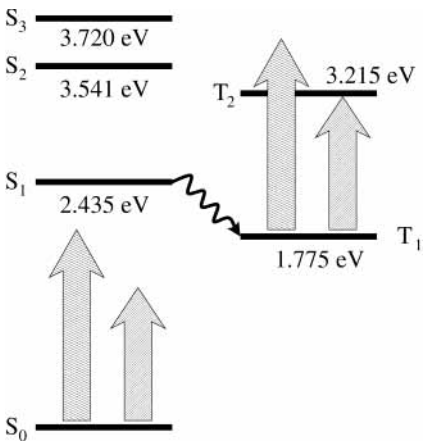

Figure 1. Zn−base porphyrin energy level diagram.

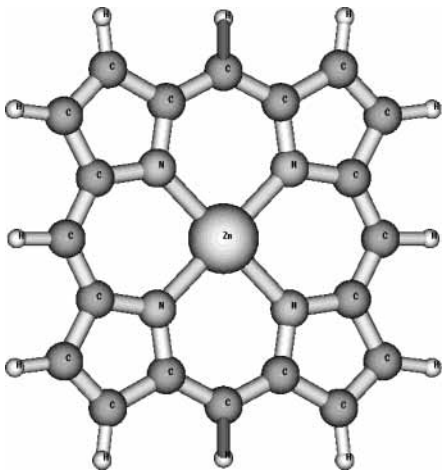

Figure 2. Zn−base porphyrin molecule (ZnP).

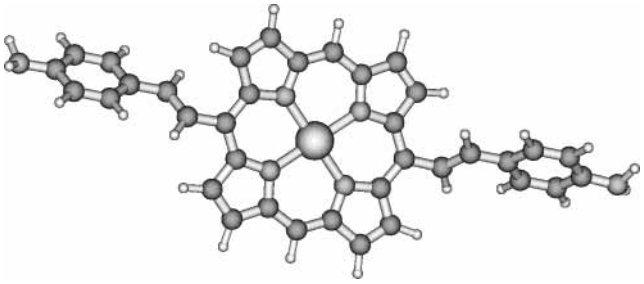

Figure 3. Vinylphenylamine Zn−base porphyrin molecule (ZnPP).

highly symmetric, without selected axes and poor charge separation, a weak nonlinear absorption is indicated. Indeed, the intensity dependence of transmission shown in Figure 5 demonstrates that the main absorption channel is off-resonant one-photon absorption. This conclusion is supported by calculations of the two-photon transition matrix elements, S_{ij},[35] collected in Table 3. For Zn−, Mg−, and Pb−base porphyrins the largest values of S_{ij} correspond to the absorption length in the interval 20−60 cm which makes the contribution of the coherent TPA process negligibly small compared with one-photon absorption.

We present in Figure 5 the transmission curves for the two-photon resonance with the S_0-S_3 transition at 1 ps pulse duration. The dependencies are the same for the two-photon resonance with the S_0-S_2 transition. A small difference, about a 20% lower value of transmission for the case presented in the figure, derives from the more efficient off-resonant one-photon absorption when the radiation frequency is tuned into the two-photon resonance with the S_0-S_3 transition—the radiation frequency is then closer to the resonant frequency of the S_0-S_2 transition. The increase of the transmission with increasing intensity is related to one-photon saturation of the absorption channels. This also evidences that the off-resonant one-photon absorption plays a major role. The lowest saturation intensity is 88 GW/cm^2 for the S_0-S_2 transition at a given pulse duration of 1 ps and $\Gamma = 0.1$ eV. The saturation intensities are much higher for other transitions; 382 GW/cm^2 for the T_1-T_2 transition, 883 GW/cm^2 for the S_1-S_3 transition, and about 3000 GW/cm^2 for the S_0-S_1 transition, and hence, the saturation effect influences strongly the S_0-S_2 transition in the chosen range of intensities.

The dependence of the transmission on Γ gives another evidence of the one-photon character of absorption. Indeed, the coherent TPA process must increase (transmission must drop down) when Γ decreases if TPA dominates.[11,18] However, Figure 5 demonstrates a gradual growth of the transmission for smaller values of the dephasing rate, $\Gamma = 0.01$ eV. The ISC rate was set to $\sim 1 \times 10^9$ s^{-1} for simulations resulting in the dashed and circled curves and to $\sim 1 \times 10^{11}$ s^{-1} for the solid curve.

It is worthwhile to remind that the pulse duration was chosen to be as short as 1 ps. As shown in refs 11 and 35 the role of stepwise incoherent many-photon processes is strongly suppressed for short pulses, while, as also well established by now, the contribution of such stepwise processes to the total nonlinear absorption cross section can be dominant if the laser pulse is sufficiently long. To check this point, we performed a set of simulations for a 100 ps pulse (see Figure 6). We then slightly decreased the frequency of radiation in order to decrease off-resonant one-photon absorption in the singlet manifold, and instead, we set the resonance to the triplet−triplet transition T_1-T_2 (see Table 2). When the rate of the inter-system crossing (ISC) between the singlet S_1 and the triplet T_1 is high enough, then an effective two-photon channel $\langle S_0|S_1\rangle\langle T_1|T_2\rangle$ appears. We made two simulations with the ISC rate set to $\sim 1 \times 10^9$ and $\sim 1 \times 10^{11}$ s^{-1}. As one can see from Table 1, the transition dipole moment between the ground state and the first excited singlet state is rather small, which gives an estimated radiative lifetime of about 0.7 μs. So, the main decay channel of this state was supposed to be the inter-system crossing.

Figure 6 (solid curve) shows a decrease of the transmission in the region of moderate (from 10 MW/cm^2 to 1 GW/cm^2) intensities when the ISC rate is equal to 1×10^{11} s^{-1}. This is because of the triplet−triplet absorption which starts to become important when the S_1 singlet state is populated. This effect is seen when the ISC rate is larger than the inverse pulse duration ($\tau^{-1} = 1 \times 10^{10}$ s^{-1}). When the ISC rate is equal to 1×10^9 s^{-1}, then the main contribution to the total absorption cross section is given by the one-photon absorption process (Figure 6, dashed curve). The growth of the transmission in the region of higher than 1 GW/cm^2 intensities owes to one-photon saturation of the T_1-T_2 and S_0-S_2 transitions. We estimated the saturation intensities of the T_1-T_2, S_0-S_1, and S_0-S_2 transitions and found them to be equal to 0.4, 104, and 11 GW/cm^2, respectively, for the given pulse duration of 100 ps. Figure 7 shows the population dynamics of the singlets S_0, S_1, and S_2 and the triplets T_1 and T_2 at an intensity of 100 GW/cm^2, which is much higher than the saturation intensities. We detect the populations at the end of the cell. As one can see the populations of the singlets S_0 and S_2 become equal as well as the populations of the triplets. Thus, the medium becomes transparent for radiation of such a high intensity, which also is reflected in the intensity dependence of the transmission.

Figure 8 shows the population dynamics of the same states at intensities lower than 1 GW/cm^2. We calculated here the populations near the entrance to the cell. The main effect is then due to the pumping of the first excited singlet state followed by the fast ISC to the first triplet state. The nonlinear absorption is quite efficient, as we can see from the intensity dependence of the transmission.

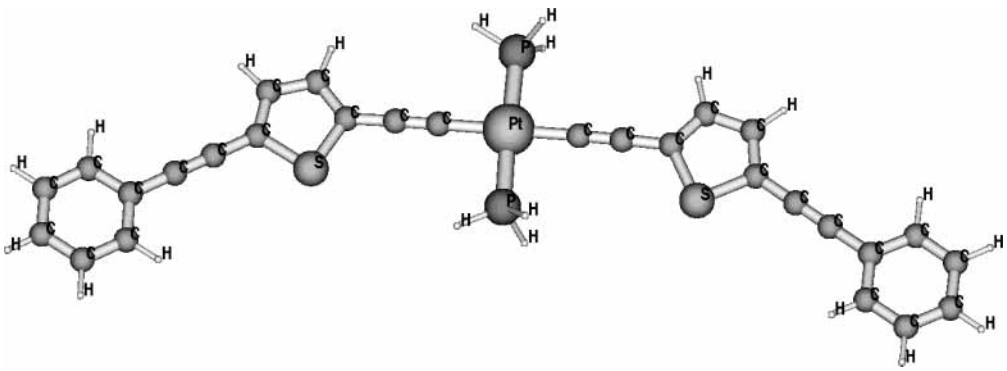

Figure 4. IVc Pt compound molecule (PtC).

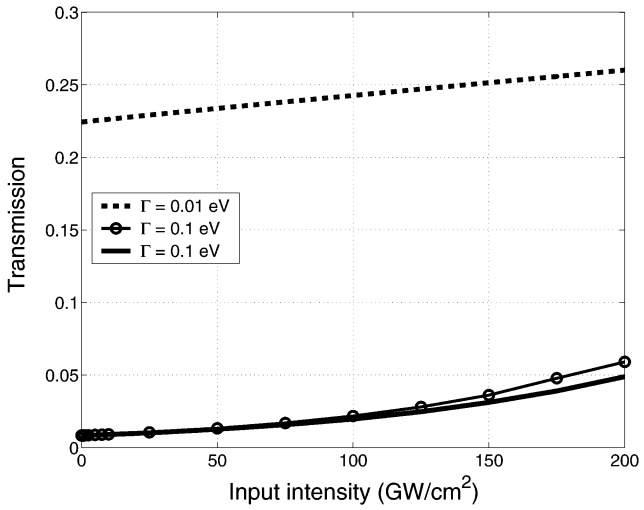

Figure 5. Transmission vs intensity for Zn−base porphyrin for different dephasing rates Γ. The difference between solid and circled lines is the inter-system crossing rate which is larger for the solid curve (see text). The pulse duration is 1 ps in all cases. Two-photon excitation is in resonance with the S_0-S_3 transition.

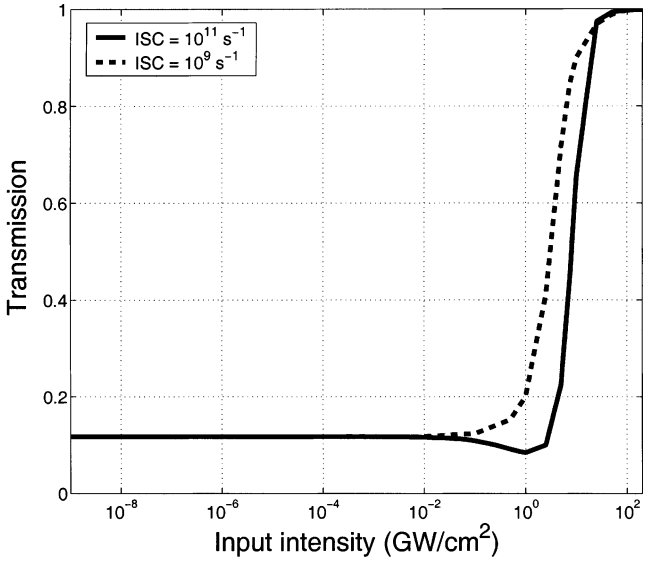

Figure 6. Transmission vs intensity for Zn−base porphyrin. The pulse duration is 100 ps. Γ = 0.1 eV. The radiation frequency is resonant to the one-photon T_1-T_2 transition.

2. Vinylphenylamine Zinc-Base Porphyrin. Our simulations of the nonlinear laser pulse dynamics for the basic metallic porphyrins showed that these compounds are not suitable for optical limiting. However, there is a way to enhance charge separation, and, hence, to gain a higher two-photon absorption cross section. That is to use different substituent groups as, for example in vinylphenylamine (Figure 3). All data for this compound are collected in Tables 1, 2, and 4. As one can see from this set of data the first excited singlet state has a very low energy which means that only infrared radiation with about 1160 nm wavelength fits a two-photon transition resonant with S_0-S_1 (see Table 1 for notations). Let us briefly analyze the possible two-photon paths as we did for the basic Zn−base porphyrin molecule. The radiation frequency should be tuned in two-photon resonance with the singlet S_1 in order to avoid the strong one-photon absorption channel S_0-S_1 arising from the large value of the transition dipole moment for this transition (see Table 1). It is necessary to say that two "real" states, 4^1S and 5^1S (see Table 1), were modeled by one effective singlet

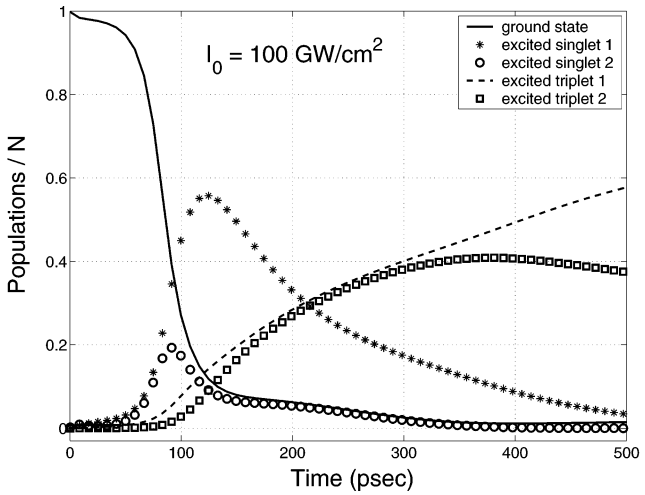

Figure 7. Population dynamics at the end of the cell at a high-intensity level. The pulse duration is 100 ps. Γ = 0.1 eV. The radiation frequency is resonant to the one-photon transition T_1-T_2.

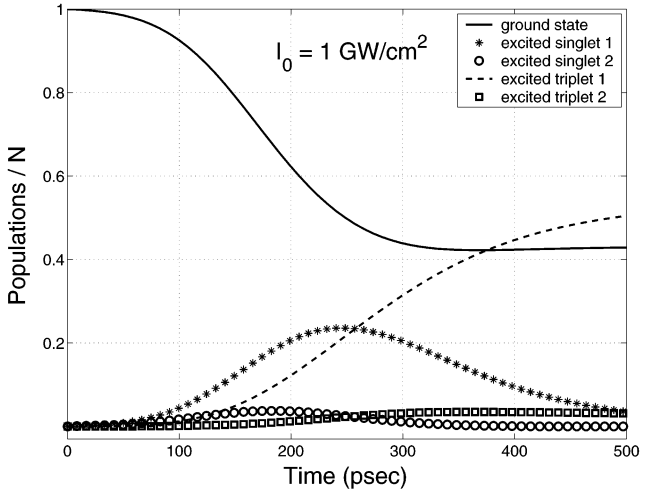

Figure 8. Population dynamics near the entrance to the cell at low intensity level. Pulse duration is 100 ps. Γ = 0.1 eV. The radiation frequency is resonant to one-photon transition T_1-T_2.

state S_3 in our simulations. The energies of these "real" states are quite close to each other and the transition dipole moment between them is very small, so it was justified to unite them in order to reduce the computational effort. The energy of the effective state is the half-sum of the energies of the original states. The dipole moment is estimated as the square root of the sum of the squared dipole moments of the original states.

According to the results of electronic structure calculations[10] there are four TPA paths starting at S_0 and finishing at S_1: $\langle S_0|S_1\rangle(\langle S_1|S_1\rangle - \langle S_0|S_0\rangle)$, $\langle S_0|S_2\rangle\langle S_2|S_1\rangle$, $\langle S_0|S_3\rangle\langle S_3|S_1\rangle$, and $\langle S_0|S_4\rangle\langle S_4|S_1\rangle$. The first channel results in weak two-photon absorption because of the small values of the permanent dipole moments of the singlets S_0 and S_1. The last three channels seem to bring about rather poor two-photon absorption because of small values of the transition dipole moments between the singlets (S_0, S_2), (S_1, S_3) and (S_1, S_4). However, there is a two-photon channel $\langle S_0|S_3\rangle\langle S_3|S_2\rangle$ which is quite intense even if we keep the two-photon resonance with the singlet S_1. The two-photon detuning is about 0.6 eV in this case which is compensated by the large values of the transition dipole moments between the singlets S_0, S_3 and S_3, S_2 (see Tables 1 and 4).

The results of the dynamics simulations at Γ = 0.01 eV are shown in Figure 9. The one-photon saturation intensity of the

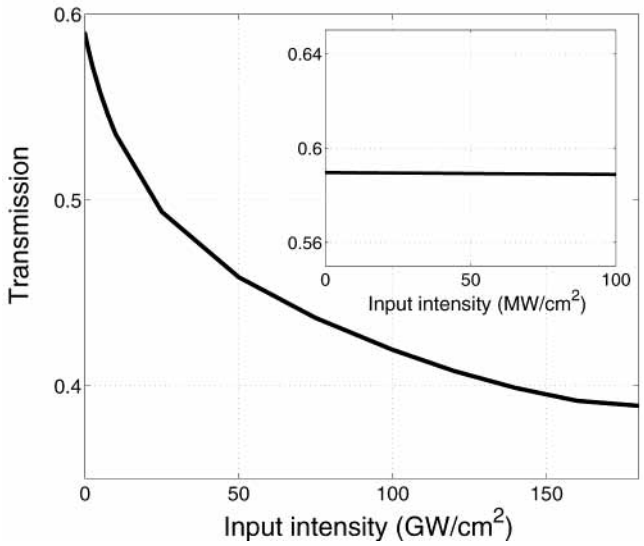

Figure 9. Transmission vs intensity for vinylphenylamine Zn−base porphyrin. Pulse duration is 1 ps. $\Gamma = 0.01$ eV. Two-photon resonance with = S_0-S_1 transition. The inset shows an almost linear regime in the region of low intensities.

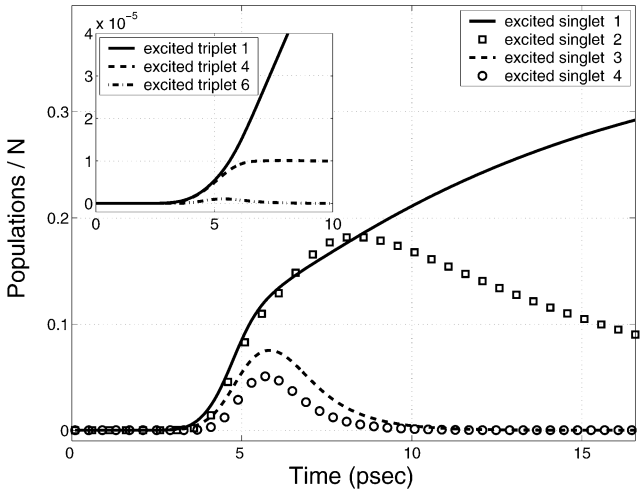

Figure 10. Population dynamics near the entrance to the cell at high-intensity level for vinylphenylamine Zn−base porphyrin. Pulse duration is 1 ps. $\Gamma = 0.01$ eV. The radiation frequency is tuned into two-photon resonance with the S_0-S_1 transition.

transition S_0-S_1 was estimated to be equal to 322 GW/cm^2 for 1 ps pulses, the same for the transition S_1-S_2 is 10.8 GW/cm^2. The transmission decreases as the intensity grows up which is a clear sign of strong two-photon absorption. On the other hand, in the region of low intensities the transmission is almost independent of intensity (see Figure 9 inset), which implies weak off-resonant linear absorption. The population dynamics presented in Figure 10 for the intensity 100 GW/cm^2 shows clearly that the main two-photon absorption channel is related to the singlet manifold of states in the case of a 1 ps pulses. As we can see from Figure 10, the contribution of the stepwise channels $\langle S_0|S_1\rangle\langle T_1|T_4\rangle$ and $\langle S_0|S_1\rangle\langle T_1|T_6\rangle$ to the total nonlinear absorption is small due to the short pulse which at the given ISC rate does not have time to pump the lowest triplet state. The ISC rate was set to 1×10^9 s^{-1} in our simulations. The saturation intensity of the triplet−triplet T_1-T_4 transition equals 2 GW/cm^2 for a 1 ps pulse according to our estimate. Such a small value is the result of an almost exact resonance of the exciting radiation with this transition. Thus, the stepwise TPA channel $\langle S_0|S_1\rangle\langle T_1|T_4\rangle$ is switched off at high intensities, especially if

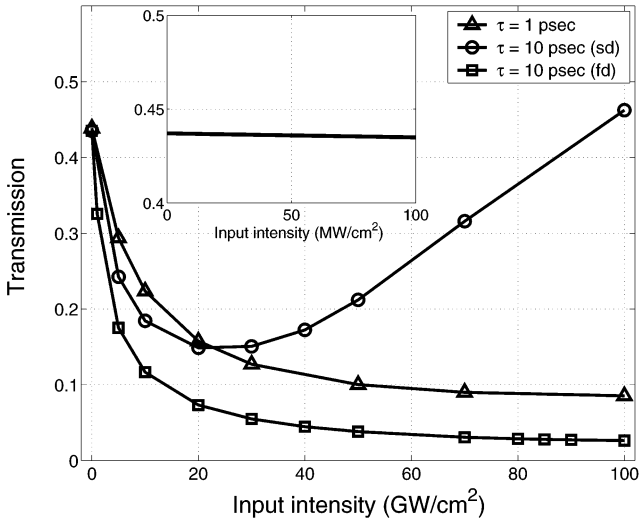

Figure 11. Transmission vs intensity for PtC at two different pulse durations. Two-photon resonance with the S_0-S_1 transition. The inset shows an almost linear regime in the region of low intensities. $\Gamma =$ 0.01 eV. "sd" = slow decay of T_4; "fd" = fast decay of T_4.

the pulse is long. In the case of a 10 ps pulse the saturation intensity of the T_1-T_4 transition constitutes 0.2 GW/cm^2. The contribution of the channel $\langle S_0|S_1\rangle\langle T_1|T_6\rangle$ to the total TPA cross section (at rather high intensities) is larger than of the channel related to the absorption to the triplet state T_4. The reason for this is that the saturation intensity for the T_1-T_6 transition is much higher—about 60 GW/cm^2 for the 1 ps pulse. It decreases slightly when the pulse is longer—40 GW/cm^2 for a 10 ps pulse. The value of the transmission at 50 GW/cm^2 initial intensity for a 10 ps pulse is 0.548 in comparison with 0.458 for a 1 ps pulse. The triplet−triplet absorption from T_1 to T_6 plays the crucial role in the case of the 10 ps pulse because the singlet−singlet S_0-S_1 transition, as well as S_1-S_2 and the triplet−triplet T_1-T_4 transitions, is saturated. The lifetime broadening of the triplet state T_4 was 1×10^{10} s^{-1} and of the triplet state T_6, 1×10^{12} s^{-1}.

3. Pt Compound (IVc). According to recent electronic structure computations the platinum-based organometallic compound IVc (Figure 4) is a very promising candidate for optical limiting. The ab initio data are collected in Tables 1, 2, and 4. As in the case of the ZnPP molecule two almost degenerate states, $4^1A'$ and $5^1A'$ (see Table 1) were modeled by one effective singlet state S_3 in our simulations for reasons described above.

The same behavior of the nonlinear transmission as in the case of ZnPP is observed for this molecule at $\tau = 1$ ps (see Figure 11, triangle-marked curve). However, the slope of the transmission is steeper for PtC. The ratio of the transmission values measured at 1 W/cm^2 and at 100 GW/c m^2, respectively, equals 5.13 in the case of PtC and 1.4 in the case of ZnPP. Off-resonant one-photon absorption is stronger for PtC in the region of small intensities ($T = 0.438$) with respect to Zn−porphyrin ($T = 0.595$). In comparison with ZnPP, this leads to more efficient nonlinear absorption in the region of high intensities due to the stepwise channels. On the other hand, the saturation intensity for the off-resonant one-photon S_0-S_1 channel becomes smaller for PtC (177 GW/cm^2 for a 1 ps pulse; see Table 8). Two-photon absorption starts to dominate one-photon absorption at intensities of about 5 GW/cm^2 (Figure 12). The theoretical curve of the two-photon absorption length ($L_{2ph} = 1/(\beta I_0)$) passes the value 0.364 cm, which corresponds to the nonsaturated one-photon absorption length at this intensity point.

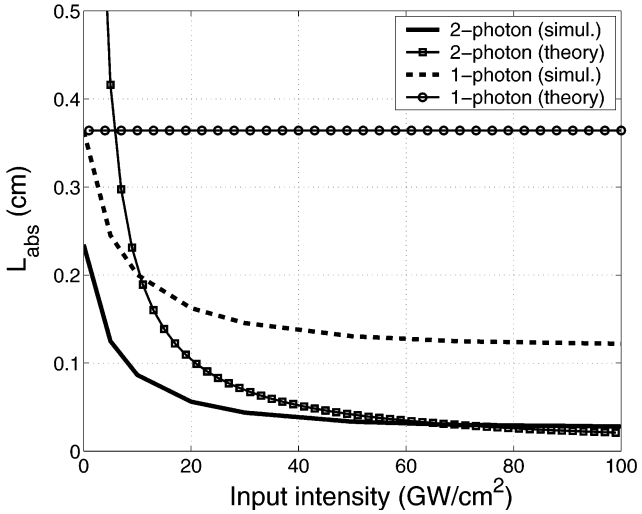

Figure 12. Absorption lengths vs intensity for the Pt compound. Pulse duration is 1 ps. $\Gamma = 0.01$ eV. Two-photon resonance with the S_0-S_1 transition. Here, "theory" means that the dependence was obtained at one particular value of the linear or two-photon absorption coefficient, while "simul." means that the dependence was obtained making use of the values of transmission at each intensity point.

TABLE 8: Saturation Intensities of Selected PtC Transitions

transition S_i-S_j	Γ_{jj}, s^{-1}	saturation intensity, GW/cm^2 $\tau = 1$ ps	$\tau = 10$ ps
S_0-S_1	10^9	177.47	17.83
S_1-S_2	10^{11}	12.12	1.82
S_1-S_3	10^{12}	3341	2112
S_2-S_3		12.32	7.79
S_0-S_3		3182	2012
T_1-T_4	10^{10}	5.20	0.54

The two-photon absorption coefficient β was estimated at $I_0 = 70$ GW/cm^2 where TPA dominates (see refs 18 and 36). As we can see from Figure 12, the simulated (calculated at each intensity value) two-photon and one-photon absorption lengths do not cross. The reason for this peculiarity is that in the region of small intensities the estimation formula[36] for the two-photon absorption length, $LT/(1 - T)$, does not apply and vice versa—in the region of high intensities the estimation of the one-photon absorption length, $-L/\ln(T)$, is not applicable.

When the pulse is long (10 ps) the transmission is high at a high-intensity level (Figure 11, circle-marked curve). On the other hand, the slope of the transmission is larger than at $\tau = 1$ ps in the region of smaller intensities—up to 10 GW/cm^2 (see Figure 11). That is because of more efficient stepwise TPA processes depending on the population of the excited singlet states.

We are now interested in the reason for such an increase of the transmission in the case of the long-pulse excitation. Apparently, the reason is saturation effects; the only question is which absorption channel is responsible for the saturation: singlet−singlet or triplet−triplet? As we mentioned above, the triplet−triplet absorption becomes important for long-pulse excitations. The saturation intensity of the T_1-T_4 transition is 0.54 GW/cm^2 for the 10 ps pulse while it is 5.2 GW/cm^2 for the 1 ps pulse (Table 8). The saturation intensity is very sensitive to the lifetime broadening of the excited state. In our case, the radiative decay rate of the excited triplet T_4 state equals approximately 1×10^9 s^{-1}. For highly excited states, the nonradiative decay processes must be of importance giving the main contribution to the total decay rate. The values of the saturation intensities (Table 8) were obtained at a 1×10^{10} s^{-1} decay rate of T_4. Such a low saturation intensity in the case of a 10 ps pulse leads to a switch-off of the effective stepwise two-photon channel $\langle S_0|S_1\rangle\langle T_1|T_4\rangle$. The population dynamics are presented in Figure 13. As we can see in Figure the transition T_1-T_4 is saturated at the 100 GW/cm^2 intensity level. A larger value of transmission—0.462 compared with 0.085 for the 1 ps pulse—signals saturation effects. However, the populations of the triplet states are low compared with the singlet states which means that the triplet−triplet absorption provides a minor contribution to the total absorption cross section at the given ISC rate (10^9 s^{-1}). As we can see from Table 8, the saturation intensities for some of the transitions in the singlet manifold of states are rather low, especially for a 10 ps pulse. It implies that the saturation will make even the singlet−singlet absorption channels less efficient at the intensities higher than 1 GW/cm^2 which in turn will increase the transmission. The population dynamics shows that the singlet−singlet transitions are saturated at a high-intensity level (Figure 13). Table 9 shows the dependence of the transmission on the ISC rate. One can see that the value of the transmission does not change much in the case of the 1 ps pulse which again implies the minor role of the triplet−triplet absorption. Such a short pulse cannot populate the singlet state S_1; therefore, the stepwise channel $\langle S_0|S_1\rangle\langle T_1|T_4\rangle$ does almost not work at all. In the case of 10 ps pulses the changes are visible although not large. It tells that the saturation of the singlet−singlet transitions is the main source of the increase of the transmission when the pulse becomes longer.

It is interesting to see what will happen if the rate of the internal conversion of the excited triplet T_4 is faster than the inverse pulse duration. We set the lifetime broadening of T_4 to 1×10^{13} s^{-1}. It results in an increase of the saturation intensity

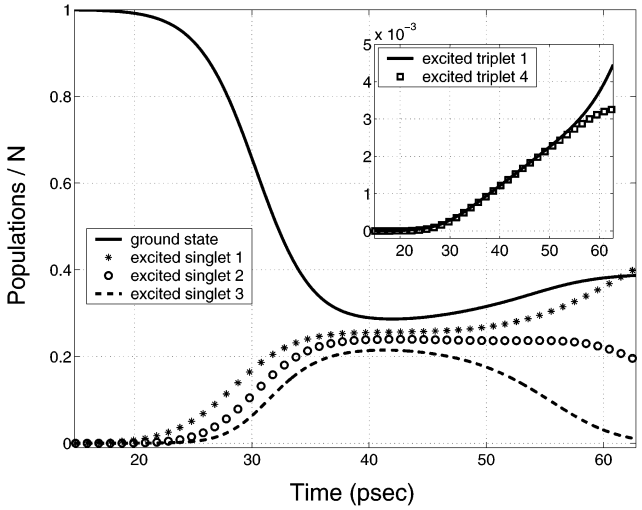

Figure 13. Population dynamics near the entrance to the cell at high-intensity level for the IVc Pt compound. Pulse duration is 10 ps. $\Gamma = 0.01$ eV. Two-photon resonance with the S_0-S_1 transition. The inset shows population dynamics of the triplet states. Slow decay of T_4.

TABLE 9: Transmission vs ISC Rate for PtC[a]

	T		
		$\tau = 10$ ps	
ISC rate, s^{-1}	$\tau = 1$ ps	$\Gamma_{T_4} = 10^{10}$ s^{-1}	$\Gamma_{T_4} = 10^{13}$ s^{-1}
10^{11}	0.0836	0.5214	0.0263
10^{10}	0.0849	0.4674	0.2272
10^9	0.0850	0.4625	0.3663
10^7	0.0850	0.4613	0.4191
10^5	0.0850	0.4612	0.4436

[a] $I_0 = 100$ GW/cm^2.

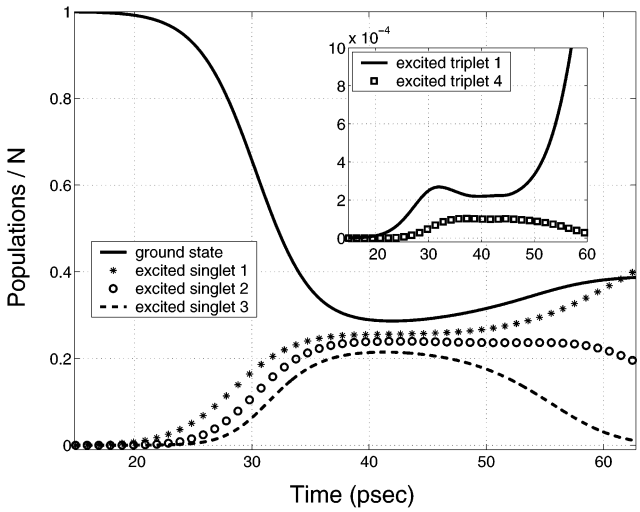

Figure 14. Population dynamics near the entrance to the cell at high-intensity level for the IVc Pt compound. Pulse duration is 10 ps. $\Gamma = 0.01$ eV. Two-photon resonance with S_0-S_1 transition. The inset shows population dynamics of the triplet states. Fast decay of T_4.

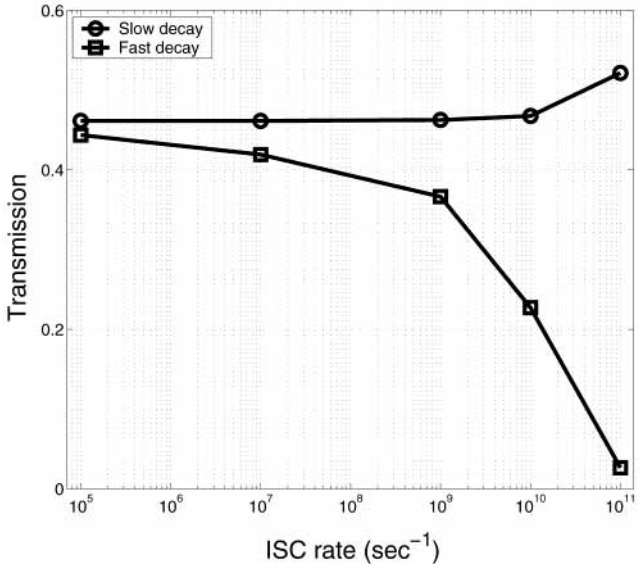

Figure 15. Dependence of the transmission on the ISC rate at different values of the decay rate of T_4 triplet state for IVc Pt compound. The pulse duration is 10 ps. $\Gamma = 0.01$ eV. $I_0 = 100$ GW/cm^2.

to the value of 52 GW/cm^2 for the 10 ps pulse. So, more efficiency than in the case of the slow decay stepwise TPA channel was expected. Indeed, the transmission dropped down to 0.366 (which though is still higher than in the case of the 1 ps pulse). The population dynamics presented in Figure 14 clearly show that the triplet−triplet transition is not saturated. Thus, the stepwise TPA channel associated with the triplet−triplet absorption can be very efficient if the ISC rate is higher than 1×10^9 s^{-1} (see Table 9 and Figure 15) or the pulse is longer than 10 ps. The square-marked curve in Figure 11 showing the transmission at the high ISC rate of 1×10^{11} s^{-1} and the fast decay of the excited triplet state T_4 proves this. However, one has to remember that the saturation intensity of the transitions is very sensitive to the pulse duration. For example, the saturation intensity of the T_1-T_4 transition decreases to 0.082 GW/cm^2 for a 100 ps pulse at the lifetime broadening of T_4 state 1×10^{10} s^{-1}. If nonradiative internal conversion makes the value of the lifetime broadening of the absorbing triplet state higher, then the saturation intensity becomes higher too and the longer pulses can be used.

V. Summary

By capitalizing on recent accomplishments in theoretical modeling in two different fields—quantum modeling of molecular excitation processes and classical computations of pulse propagation—we are in a position to address detailed issues concerning optical power limiting as well as to obtain a more holistic picture why certain compounds are effective in this respect. We illustrate these possibilities by presenting simulation results for a couple of organometallic compounds that are believed to be potential optical limiters. Electronic structure calculations were thus carried out for basic metal−base porphyrins, for vinylphenylamine porphyrin, and for the type IVc platinum compound aiming at a characterization of their electronic properties related to nonlinear absorption of electromagnetic radiation. A comparative analysis of the optical limiting capability of those molecules was performed based on dynamical simulations of nonlinear pulse propagation. The total transmission vs pulse intensity and pulse length was thus predicted for these compounds and several key features and rate-limiting steps in the transmission were pinpointed.

We showed that the type IVc platinum compound exhibits better optical limiting properties than porphyrins for short-pulse excitations. The special design of this compound such as triple C−C bonds shifting the energy of the first excited singlet state, and phenyl and thiophene groups providing enhanced nonlinear optical response contributes to a large apparent TPA cross section. On the other hand, the large value of the transition dipole moment between the triplet states and close to resonant conditions between the exciting radiation and a triplet−triplet transition results in a low saturation intensity of this transition leading to a decrease of efficiency of the stepwise TPA channel associated with inter-system crossing. Thus, the saturation effects can easily spoil the optical limiting capability if the exciting pulses are long—the critical pulse length evidently being different for different compounds. The saturation intensity is quite sensitive to the nonradiative quenching and hence to the lifetime broadening of the higher triplet state. The high nonradiative internal conversion rate of the higher triplet states results in a large value of the saturation intensity. In this case, the upper limit of the pulse duration allowing for an efficient optical limiting is shifted toward longer than 10 ps pulses for the IVc platinum compound. The ISC rate has anyway to be comparable with the inverse pulse duration in order to boost the stepwise TPA channel associated with the singlet−singlet transition followed by a triplet−triplet transition. This suggests that organometallic compounds, especially those containing heavy elements, are good candidates for optical limiting as the "heavy atom effect" with large spin−orbit coupling produces strong mixing between S_1 and T_1. As the spin−orbit coupling grows as the third power with the effective nuclear charge one can thus easily predict that platinum elements are better than the zinc elements for optical limiting, all other factors unaccounted. However, it may be that a very effective inter-system crossing just shifts the rate-limiting step further down the chain of process—to triplet−triplet absorption, and, in particular, to the quenching of the upper triplet states. From the computational point of view we have demonstrated that response theory is effective in estimating the S_1-T_1 coupling—as residues of a quadratic response functions—but we note also as this interaction does not involve particle exchange and is degenerate, it must be strongly driven by vibronic interactions; the spin−orbit coupling serving only as an "electronic prefactor".

The above statements are supported by an analysis of population dynamics performed for different values of the

lifetime broadening of the higher triplet state. As a matter of fact, the singlet−singlet absorption channels appeared to be easily saturable too at pulse durations longer than 10 ps and the stepwise TPA associated with those channels do not contribute to the total TPA cross section at the intensities higher than the lowest saturation intensity. All of this leads to an increase of the transmission, and hence worse optical limiting if the ISC rate is less than the inverse pulse duration.

On the basis of results received, we can say that the structure-to-property relations of the rate-limiting steps (properties) must serve as important criteria for successful choices of a compound suitable for the application of interest. For instance, the low energy and charge-transfer character of the first excited singlet state of vinylphenylamine porphyrin makes this compound suitable for up-conversion of infrared radiation which is of importance for biomedical applications, while the IVc platinum compound with the strong inter-system crossing seems to be the good optical limiter among those compounds investigated. Basic metal−base porphyrins exhibit strong off-resonant linear absorption dominating all nonlinear absorption channels at least for shorter than 100 ps pulses. Excitation by longer pulses results in an intense TPA associated with inter-system crossing if the ISC rate is comparable with the inverse pulse duration. However, the saturation of the triplet−triplet transitions makes such media transparent at rather moderate intensities of the exciting radiation.

Finally, it is important to stress that modeling of nonlinear pulse propagation at high intensities of incident fields suffer from shortcomings if the conventional expansion of the nonlinear polarization over powers of the electric field strength is employed. In this case not only the saturation effects are treated poorly but so also the coupling of different multiphoton processes, resulting in neglect of leading terms in the nonlinear polarization. The present general methodology transcends the power expansion approach and thus overcomes its limitations.

Acknowledgment. We acknowledge a grant from the photonics project run jointly by the Swedish Materiel Administration (FMV) and the Swedish Defense Research Agency (FOI). The authors also acknowledge support from the Swedish Research council (VR).

References and Notes

(1) Chung, S.-J.; Kim, K.-S.; Lin, T.-C.; He, G. S.; Swiatkiewicz, J.; Prasad, P. N. *J. Phys. Chem. B* **1999**, *103*, 10741−10745.

(2) He, G. S.; Swiatkiewicz, J.; Jiang, Y.; Prasad, P. N.; Reinhardt, B. A.; Tan, L.-S.; Kannan, R. *J. Phys. Chem. A* **2000**, *104*, 4805−4810.

(3) He, G. S.; Yuan, L.; Cheng, N.; Bhawalkar, J. D.; Prasad, P. N.; Brott, L. L.; Clarson, S. J.; Reinhardt, B. A. *J. Phys. Chem. A* **1997**, *14*, 1079−1087.

(4) Parthenopoulos, D. A.; Rentzepis, P. M. *Science* **1989**, *245*, 843−845.

(5) Denk, W.; Strickler, J. H.; Webb, W. W. *Science* **1990**, *248*, 73−76.

(6) Strickler, J. H.; Webb, W. W., Antos, R. L.; Krisiloff, A. J., Eds.; *Proc. SPIE* **1991**, *1398*, 107−117.

(7) Bhawalkar, J. D.; Kumar, N. D.; Zhao, C. F.; Prasad, P. N. *J. Clin. Laser Med. Surg.* **1997**, *15*, 201−204.

(8) He, G. S.; Markowicz, P. P.; Lin, T.-C.; Prasad, P. N. *Nature (London)* **2002**, *415*, 767−770.

(9) Nguyen, K. A.; Pachter, R. *J. Chem. Phys.* **2003**, *118*, 5802−5810.

(10) Norman, P.; Cronstrand, P.; Ericsson, J. *Chem. Phys.* **2002**, *285*, 207−220.

(11) Baev, A.; Gel'mukhanov, F.; Rubio-Pons, O.; Cronstrand, P.; Ågren, H. *J. Opt. Soc. Am. B* **2004**, *21*, 384−396.

(12) Tunnell, I.; Rinkevicius, Z.; Salek, P.; Vahtras, O.; Helgaker, T.; Ågren, H. *J. Chem. Phys.* **2003**, *119*, 11024−11034.

(13) Nguyen, K. A.; Day, P. N.; Pachter, R.; Tretiak, S.; Chernyak, V.; Mukamel, S. *J. Phys. Chem. A* **2002**, *106*, 10285−10293.

(14) Norman, P.; Luo, Y.; Ågren, H. *J. Chem. Phys.* **1999**, *111*, 7758−7765.

(15) Frisch, M. J.; Trucks, G. W.; Schlegel, H. B.; Scuseria, G. E.; Robb, M. A.; Cheeseman, J. R.; Zakrzewski, V. G.; Montgomery, J. A., Jr.; Stratmann, R. E.; Burant, J. C.; Dapprich, S.; Millam, J. M.; Daniels, A. D.; Kudin, K. N.; Strain, M. C.; Farkas, O.; Tomasi, J.; Barone, V.; Cossi, M.; Cammi, R.; Mennucci, B.; Pomelli, C.; Adamo, C.; Clifford, S.; Ochterski, J.; Petersson, G. A.; Ayala, P. Y.; Cui, Q.; Morokuma, K.; Malick, D. K.; Rabuck, A. D.; Raghavachari, K.; Foresman, J. B.; Cioslowski, J.; Ortiz, J. V.; Stefanov, B. B.; Liu, G.; Liashenko, A.; Piskorz, P.; Komaromi, I.; Gomperts, R.; Martin, R. L.; Fox, D. J.; Keith, T.; Al-Laham, M. A.; Peng, C. Y.; Nanayakkara, A.; Gonzalez, C.; Challacombe, M.; Gill, P. M. W.; Johnson, B. G.; Chen, W.; Wong, M. W.; Andres, J. L.; Head-Gordon, M.; Replogle, E. S.; Pople, J. A. *Gaussian 98*, revision A.9; Gaussian, Inc.: Pittsburgh, PA, 1998.

(16) Helgaker, T.; Jensen, H. J. Aa.; Jorgensen, P.; Olsen, J.; Ruud, K.; Ågren, H.; Andersen, T.; Bak, K. L.; Bakken, V.; Christiansen, O.; Dahle, P.; Dalskov, E. K.; Enevoldsen, T.; Heiberg, H.; Hettema, H.; Jonsson, D.; Kirpekar, S.; Kobayashi, R.; Koch, H.; Mikkelsen, K. V.; Norman, P.; Packer, M. J.; Saue, T.; Taylor, P. R.; Vahtras, O. *Dalton, an ab initio electronic structure program* (Release 1.0, 1997). See http://www.kjemi.uio.no/software/dalton/dalton.html.

(17) Widmark, P.-O.; Malmqvist, P. Å.; Roos, B. O. *Theor. Chem. Acc.* **1990**, *77*, 291−306.

(18) Baev, A.; Gel'mukhanov, F.; Kimberg, V.; Ågren, H. *J. Phys. B: At. Mol. Opt. Phys.* **2003**, *36*, 3761−3774.

(19) Gouterman, M. *J. Mol. Spectrosc.* **1961**, *6*, 138.

(20) Langhoff, S. R.; Davidson, E. R.; Kern, C. W. *J. Chem. Phys.* **1975**, *63*, 4800.

(21) Nakatsuji, H.; Hasegawa, J.; Hada, M. *J. Chem. Phys.* **1996**, *104*, 2321.

(22) Hasegawa, J.; Ozeki, Y.; Hada, M.; Nakatsuji, H. *J. Phys. Chem. B* **1998**, *102*, 1320.

(23) Sundholm, D. *Chem. Phys. Lett.* **1999**, *302*, 480.

(24) Sundholm, D. *Phys. Chem. Chem. Phys.* **2000**, *2*, 2275−2281.

(25) Sundholm, D. *Chem. Phys. Lett.* **2000**, *317*, 392−399.

(26) Parusel, A. B. J.; Grimme, S. *J. Porphyrins Phthalocyanines* **2001**, *5*, 225.

(27) Ohkawa, K.; Hada, M.; Nakatsuji, H. *J. Porphyrins Phthalocyanines* **2001**, *5*, 256.

(28) Rubio, M.; Roos, B. O.; Serrano-Andrés, L.; Merchán, M. *J. Chem. Phys.* **1999**, *110*, 7202−7209.

(29) Serrano-Andrés, L.; Merchán, M.; Rubio, M.; Roos, B. O. *Chem. Phys. Lett.* **1998**, *295*, 195−203.

(30) Bauernschmitt, R.; Ahlrichs, R. *Chem. Phys. Lett.* **1996**, *256*, 454.

(31) van Gisbergen, S. J. A.; Rosa, A.; Ricciardi, G.; Baerends, E. J. *J. Chem. Phys.* **1999**, *111*, 2499−2506.

(32) Nguyen, K. A.; Day, P. N.; Pachter, R. *J. Phys. Chem. A* **2000**, *104*, 4748−4754.

(33) Clarke, R. H. *Triplet State ODMR Spectroscopy*; John Wiley and Sons: New York, Chichester, England, Toronto, Canada, and Singapore, 1982.

(34) Macak, P.; Luo, Y.; Ågren, H. *Chem. Phys. Lett.* **2000**, *330*, 447−456.

(35) Gel'mukhanov, F.; Baev, A.; Macak, P.; Luo, Y.; Ågren, H. *J. Opt. Soc. Am. B* **2002**, *19*, 937−945.

(36) Baev, A.; Gel'mukhanov, F.; Macak, P.; Luo, Y.; Ågren, H. *J. Chem. Phys.* **2002**, *117*, 6214−6220.

(37) Loboda, O.; Tunell, I.; Minaev, B.; Ågren, H. *J. Phys. Chem.*, to be published 2004.